AMERICAN SOCIETY FOR MICROBIOLOGY | Infection and Immunity

ALL2, a Homologue of *ALL1*, Has a Distinct Role in Regulating pH Homeostasis in the Pathogen *Cryptococcus neoformans*

Neena Jain,[a] Tejas Bouklas,[b] Anjali Gupta,[a] Avanish K. Varshney,[b] Erika P. Orner,[c] Bettina C. Fries[b,c]

Department of Medicine (Infectious Diseases), Albert Einstein College of Medicine, Bronx, New York, USA[a]; Departments of Medicine (Infectious Diseases)[b] and Microbiology and Molecular Genetics,[c] Stony Brook University, Stony Brook, New York, USA

***Cryptococcus neoformans* is a facultative intracellular fungal pathogen that has a polysaccharide capsule and causes life-threatening meningoencephalitis. Its capsule, as well as its ability to survive in the acidic environment of the phagolysosome, contributes to the pathogen's resilience in the host environment. Previously, we reported that downregulation of allergen 1 (*ALL1*) results in the secretion of a shorter, more viscous exopolysaccharide with less branching and structural complexity, as well as altered iron homeostasis. Now, we report on a homologous coregulated gene, allergen 2 (*ALL2*). *ALL2*'s function was characterized by generating null mutants in *C. neoformans*. In contrast to *ALL1*, loss of *ALL2* attenuated virulence in the pulmonary infection model. The *all2*Δ mutant shed a less viscous exopolysaccharide and exhibited higher sensitivity to hydrogen peroxide than the wild type, and as a result, the *all2*Δ mutant was more resistant to macrophage-mediated killing. Transcriptome analysis further supported the distinct function of these two genes. Unlike *ALL1*'s involvement in iron homeostasis, we now present data on *ALL2*'s unique function in maintaining intracellular pH in low-pH conditions. Thus, our data highlight that *C. neoformans*, a human-pathogenic basidiomycete, has evolved a unique set of virulence-associated genes that contributes to its resilience in the human niche.**

Cryptococcus neoformans is a major fungal pathogen that causes disease predominantly in patients with AIDS but also in patients with other immune deficiencies. The most common clinical presentation of cryptococcal disease is chronic meningoencephalitis (CME). Worldwide, approximately 1 million new cases of cryptococcal meningitis occur every year, resulting in more than 600,000 deaths (1). Despite advances made in antifungal treatment, intracranial pressure management, and antiretroviral therapy, there is a major challenge to rapidly clear *C. neoformans* from cerebral spinal fluid (CSF), which is required to achieve a good outcome (2). The pathogen has various highly regulated virulence traits, including capsule, melanin formation, growth at 37°C, and extracellular enzymes (3). Differential gene regulation of these virulence traits can promote microevolution *in vivo*, which may facilitate evasion of the host immune response. One process by which microevolution can be achieved is phenotypic switching, which generates variants with augmented virulence that also alter host-pathogen interactions (4, 5).

In our previous studies, we documented that RC2, a serotype D *C. neoformans* clinical strain that is also a standard laboratory strain (6), undergoes phenotypic switching from a smooth to mucoid colony morphology and is associated with downregulation of a defined set of genes, including allergen 1 (*ALL1*) (7). Loss of *ALL1* function resulted in a hypervirulent phenotype in both serotype A- and D-null mutants (*all1*Δ). Furthermore, it was shown that *ALL1* is regulated during capsule induction (8) and by the transcription factor Sp1 and the *PKC1* gene under glucose starvation (9), as well as by *CIR1* in response to changes in iron concentration (10). Under starvation, *VAD1* downregulates *ALL1* transcripts via degradation of mRNA (11). Although the precise function of *ALL1* is not known, its expression indirectly affects polysaccharide conformation and iron homeostasis (12). Thus, intracisternal infection with the *all1*Δ mutant results in augmented intracerebral pressure and premature death in infected rats (7). Extensive homology search for *ALL1* revealed a highly homologous uncharacterized cryptococcal gene, CNM02200 (JEC21), which was subsequently named *ALL2*. Similarly to *ALL1*, *ALL2* is also regulated by Sp1 and *PKC1* under glucose starvation and during capsule induction (9).

In the present study, we sought to characterize the function of this gene and generated a null mutant of *ALL2* (*all2*Δ) and a double mutant of *ALL1* and *ALL2* (*all1*Δ *all2*Δ). Results obtained imply that these homologous genes differ in their contribution to virulence and associated function. In contrast to the loss of *ALL1*, the loss of *ALL2* attenuates virulence, and the mutants shed more of a less viscous exopolysaccharide (exo-PS). Microarray analysis supports distinct functions for these homologous genes and indicates that, unlike *ALL1*, the gene *ALL2* is involved in maintaining intracellular pH.

MATERIALS AND METHODS

Yeast strains and media. The *C. neoformans* strains used in this study are listed in Table S1 in the supplemental material. *C. neoformans* strains were cultured at 37°C in YNB broth (0.67% yeast nitrogen base without amino acids plus 2% glucose) or grown on YPD broth/agar (20 g/liter glucose, 10 g/liter yeast extract, 20 g/liter peptone [for YPD agar, 20 g/liter agar was

Received 10 August 2015 **Returned for modification** 24 August 2015
Accepted 13 November 2015

Accepted manuscript posted online 23 November 2015

Citation Jain N, Bouklas T, Gupta A, Varshney AK, Orner EP, Fries BC. 2016. *ALL2*, a homologue of *ALL1*, has a distinct role in regulating pH homeostasis in the pathogen *Cryptococcus neoformans*. Infect Immun 84:439–451. doi:10.1128/IAI.01046-15.

Editor: G. S. Deepe, Jr.

Address correspondence to Bettina C. Fries, bettina.fries@stonybrookmedicine.edu.

Supplemental material for this article may be found at http://dx.doi.org/10.1128/IAI.01046-15.

added]), unless otherwise stated. For glucose starvation studies, YNB broth supplemented with 0.2% glucose, no glucose, or asparagine salt medium (1 g/liter asparagine, 10 mM sodium phosphate [pH 6.5], and 0.25 g/liter $MgSO_4$) was used. For screening mutants, YPD supplemented with 100 mg/liter nourseothricin (*NAT*) or 200 mg/liter neomycin G418 (*NEO*) was used. RNA for microarray analysis was isolated from *C. neoformans* cells grown in minimal medium (10 mM magnesium sulfate, 29.3 mM potassium phosphate monobasic, 13 mM glycine, and 3 μM thiamine-HCl; adjusted to pH 5.5 and supplemented with 15 mM glucose as the carbon source). Other relevant media are specified below.

Strain construction. The *C. neoformans* serotype A and D reference sequences were accessed originally through TIGR (now available at the NCBI) and the Fungal Genome Initiative database at the Broad Institute (http://www.broadinstitute.org/annotation/genome/cryptococcus_neoformans/MultiHome.html).

Generation of *all2*Δ, *all2*Δ+P_{ACT1}-*ALL2*, and *all1*Δ *all2*Δ mutants. The *ALL2* gene is 1,549 bp long, has four introns, and encodes a putative protein with a molecular mass of 25 kDa. In strain JEC21, *ALL2* (CNM02200) is located on chromosome 13. To generate the *all2*Δ mutant, the coding region of *ALL2* (RC2, 926 bp) was replaced with a neomycin resistance marker by homologous recombination as described previously (7). Primers used to generate mutants are listed in Table S2 in the supplemental material. Homologous recombination was confirmed by PCR, Southern blot analysis, and real-time PCR of *ALL2* transcripts. For *ALL2* complementation, the *ACT1* promoter and the *ALL2* open reading frame (ORF) were amplified from genomic DNA of RC2 and fused in frame using the NdeI restriction site. *ACT1* and *ALL2* fragments were cloned in pJAF13 using XbaI and XhoI cloning sites to generate plasmid pJAF13/P_{ACT1}-*ALL2*. The plasmid pJAF13/P_{ACT1}-*ALL2* was linearized by XhoI and introduced into the *all2*Δ mutant by biolistic transformation. *ALL2*-positive clones (*all2*Δ+P_{ACT1}-*ALL2*) were selected on YPD agar with 100 mg/liter *NAT*. Gene complementation was confirmed by PCR, and the level of *ALL2* expression was determined by reverse transcription-PCR (RT-PCR) of *ALL2* transcripts. For generation of the *all1*Δ *all2*Δ double mutant, the *ALL1* gene was replaced with the *NAT* resistance marker in RC2-*all2*Δ by modifying the construct designed previously to disrupt *ALL1* (7). Positive clones were selected on YPD agar containing 100 mg/liter *NAT* and 200 mg/liter *NEO*. Homologous recombination was confirmed by PCR, Southern blot analysis, and determining the transcription level of *ALL1* and *ALL2* by RT-PCR.

Phenotypic characterization. Mutants were phenotypically characterized for (i) baseline and induced capsule size, (ii) growth rate in variable pH and Dulbecco's modified Eagle's medium (DMEM) supplemented with 10% fetal calf serum, 10% NCTC, 1% nonessential amino acids, 1% penicillin-streptomycin, or minimal medium (10 mM magnesium sulfate, 29.3 mM potassium phosphate monobasic, 13 mM glycine, 3 μM thiamine-HCl; adjusted to pH 5.5 and supplemented with 15 mM glucose as the carbon source), (iii) *in vitro* stress sensitivity (1 M potassium chloride, lithium chloride [100 and 200 mM with glucose and galactose, respectively], 1 M sodium chloride), (iv) hydrogen peroxide sensitivity, (v) macrophage phagocytosis index, and (vi) macrophage-mediated killing assays as described previously (13–16). The intrinsic viscosity of exopolysaccharide and glucuronic acid residue content was determined as previously described (17, 18). All measurements were done in triplicate.

Generation of *ALL1*::HA-tagged and *ALL2*:mCherry fusion protein strains. The *ALL1*::HA-tagged strain (where HA is hemagglutinin) was generated using the following strategy (19, 20). The *ALL1* gene was amplified under its own promoter from RC2 genomic DNA using primers ALL1-prom-F-XbaI and ALL1-HARev (see Table S2 in the supplemental material). The resulting fragment and pJAF1 were digested with XbaI and NcoI and ligated to generate the 5′*ALL1*-HA/pJAF1 construct. The 3′ untranslated region (3′UTR) of the *ALL1* gene was cloned in frame behind *ALL1*-HA using EcoRV and NcoI to generate 5′*ALL1*-HA/3′UTR/pJAF1. Next, 1,000 bp downstream of *ALL1* was cloned into *ALL1*-HA/3′UTR/pJAF1 using the restriction sites for BamHI and KpnI to generate 5′*ALL1*-HA/3′UTR/*NEO*/*ALL1*-3′pJAF1. The construct was restricted with XbaI and KpnI, yielding a linearized fragment of 5′*ALL1*-HA/3′UTR/*NEO*/*ALL1*-3′, which was biolistically delivered into RC2 using a standard procedure as described previously (7). Homologous recombination was confirmed by PCR. *ALL1*::HA was detected by Western blot hybridization using rabbit anti-HA polyclonal antibody and a chemiluminescence kit (Pierce/Life Technologies) according to the manufacturer's instructions.

To generate *ALL2*-mCherry fusion protein in *ALL1*::HA strain for localization studies, plasmid YP164 (a generous gift from the Peter Williamson lab) was used to express a fusion between *ALL2* and a synthetic mCherry protein (21). *ALL2* under *ACT1* promoter was amplified from previously generated plasmid P_{ACT1}-*ALL2*/pJAF13 using primers All2For-NHEI and All2Rev-PST1 and inserted into the plasmid YP164 using standard cloning techniques to generate plasmid *ALL2*/mCherry/YP142. Further, ALL2-mCherry was amplified from plasmid *ALL2*/mCherry/YP142 using the primers P_{Act}-XbaFor and mCherry rev-EcoRV, and *ALL2*-3′UTR was amplified from RC2-SM genomic DNA using the primers All2 3′UTR-For ECORV and All2 3′UTR-Rev XHOI. Both parts were cloned in frame in plasmid pJAF13 using standard cloning techniques. The plasmid *ALL2*/mCherry/3′UTR/pJAF13 was linearized and transformed in *ALL1*::HA cells using the standard biolistic transformation technique.

All1p and All2p localization *in vivo*. For localization studies, immunofluorescence was performed as described previously (20) with few modifications. Briefly, RC2 wild-type (RC2-wt) cells for All1p::HA and All2p-mCherry were cultured for 16 h in YNB up to an optical density at 600 nm of 0.4 to 0.5. Cells were harvested by centrifugation (5,000 rpm for 1 min), washed once with phosphate-buffered saline (PBS), suspended in 1 ml of 4% paraformaldehyde in PBS, and incubated for 30 min with rotation. The sample was then washed three times with PBS, suspended in 1 ml of lysis buffer (50 mM sodium citrate [pH 6.0], 1 M D-sorbitol, 35 mM β-mercaptoethanol) plus 40 mg/ml lysing enzyme (from *Trichoderma harzianum*), and incubated for 1 to 2 h at 37°C with occasional inversion. To monitor the protein mobility in variable growth phase, the cells were harvested at different time points during the experiment. After digestion, the cells were washed twice with heparan sulfate (HS) buffer (100 mM HEPES [pH 7.5], 1 M D-sorbitol) and suspended in 200 μl of HS buffer. The washed cell pellet was incubated with HS buffer containing 1% Triton X-100 and incubated for 10 min; it was then washed three times with HS buffer and three times with PBS. Next, the cells were treated with blocking buffer (5% goat serum and 0.02% Triton X-100 in PBS) for 1 h, followed by a high-affinity rabbit anti-HA polyclonal antibody (1:250/1:500 in blocking buffer [BB] obtained from Roche Applied Science) at 4°C in a rotator. Samples were then washed six times with blocking buffer and stained with Alexa Fluor 594-goat anti-rabbit IgG (1 μg/ml in BB) for 1 h in the dark. The cells were washed three times with BB and three times with PBS. Bright-field and fluorescence images were acquired as for the capsule staining assays described above.

Murine virulence studies. BALB/c mice (female, 6 to 8 weeks old) were obtained from the National Cancer Institute (Bethesda, MD). Mice ($n = 10$ per group) were infected intratracheally (i.t.) with 5×10^4 or intravenously (i.v.) with 10^6 of wild type (RC2) or respective mutant cells in PBS. Mouse health was monitored daily, and if moribund, the mice were sacrificed in accordance with Institutional Animal Care and Use Committee (IACUC) regulations at the Albert Einstein College of Medicine (AECOM). To determine CFU studies, infected mice were killed at day 7 or 14, and their lungs were excised. Half of the lung was plated for CFU, and the other half was fixed in 10% formalin for histological analysis. Lung tissues were stained with hematoxylin and eosin, as well as mucicarmine, by the Histopathology Core at AECOM and Stony Brook University. Survival curves were generated and analyzed using GraphPad Prism 6.0.

***ALL2* expression in glucose starvation.** RC2 cells were grown overnight in YNB supplemented with 2% glucose, diluted 1:50, and then again grown for 8 h in YNB supplemented with 2% glucose, 0.2% glucose, or no

glucose. RNA transcript levels were measured by RT-PCR as previously described (7) in a 10-μl reaction mixture containing SYBR green master mix (Applied Biosystems/Life Technologies) with the primers listed in Table S2 in the supplemental material. An RT-PCR analysis was performed with the appropriate controls, and the relative transcript levels were determined as described earlier (12).

Microarray and GO enrichment analysis. RC2-wt and mutant cells were grown in minimal medium for 16 h at 37°C with agitation (150 rpm), diluted 1:100, and regrown for 16 h or up to an optical density of 0.6 to 0.7 with agitation (150 rpm) at 37°C. Experiments were performed in duplicates (minimal medium arrays). Total RNA was isolated, and the microarray was performed by the Genome Technology Access Center at Washington University in St. Louis. Microarray analysis and gene ontology (GO) enrichment analysis were performed by the facility as described previously (12). Microarray results were further confirmed by performing RT-PCR on select genes as described above. A functional network was generated using Cryptonet (http://www.inetbio.org/cryptonet/).

Measurement of vacuolar pH. Intracellular pH (pH_i) of cells grown in YNB with variable glucose, as well as total pH, was measured using the pH-sensitive fluorophore BCECF-AM [2′7′-bis-(2-carboxyethyl)-5-(and 6)-carboxyfluorescein]. BCECF accumulates in yeast vacuoles, and excitation spectra are sensitive to pH (22). pH_i measurement was performed by collecting the ratio of fluorescence at two excitation wavelengths (450 and 490 nm) and measuring at a single emission wavelength (535 nm) using protocols described elsewhere (23).

ATP measurement. Cellular ATP levels were measured as previously described (24). Briefly, cells were grown in 50 ml of YNB buffered with 50 mM MES (morpholineethanesulfonic acid) (pH 4 and pH 7) for 16 h with constant agitation of 150 rpm at 37°C. The cultures were centrifuged at 3,000 rpm for 10 min to collect the pellet and washed once with PBS. The cells were counted using a hemocytometer, and a pellet of a similar number of cells was suspended in 1 ml of 50 mM HEPES (pH 7). The cells were further disrupted with a bead-beater (Biospec Products) using prewashed 0.5-mm zirconia beads. Disrupted samples were centrifuged at 8,000 rpm at 4°C for 10 min. The ATP concentrations of supernatants were determined using an ATP bioluminescence assay kit (Sigma-Aldrich, St. Louis, MO). ATP concentrations were normalized with total protein concentrations for each sample. The mean measurements for triplicate samples were reported.

Chronological and replicative life spans. The chronological life span (CLS) was determined by adaptation of *Saccharomyces cerevisiae* methods (25) with some modifications. Briefly, equal numbers of *C. neoformans* cells were grown in YNB medium with or without 2% dextrose for 3 days at 37°C until they reached stationary phase. The cells were then transferred to sterile-distilled H_2O, and the number of viable cells was measured by plating appropriate dilutions every 2 to 3 days on Sabouraud dextrose agar (SDA) plates. CFU on the plates were quantitated at 48 h, and the study was terminated when 99% of the cells were dead. All measurements were performed in triplicates.

The replicative life span (RLS) was determined by microdissection using a tetrad dissection Axioscope A1 microscope (Zeiss) as described previously in *S. cerevisiae* (26) with some modifications for *C. neoformans*. Briefly, the first buds of *C. neoformans* cells ($n = 20$ to 40) were arrayed on a YPD agar plate maintained at 37°C and then evaluated every 1 to 2 h by separating newly arising buds using a 50-μm fiber optic needle (Cora Styles). The RLS of each cell was calculated by determining the sum of the total buds until the cessation of divisions.

Statistical analysis. Statistical analysis, including Student's *t* test, Wilcoxon rank sum test, and log-rank test, was performed using Microsoft Excel 2011 and GraphPad Prism 6.0 for Macintosh.

Microarray data accession number. Microarray data for the mutant and the wt were uploaded to the GEO database and assigned GEO accession no. GSE74219.

RESULTS

Identification of *ALL2* and generation of *all2*Δ and *all1*Δ *all2*Δ mutants. The *ALL2* gene is highly conserved among *C. neoformans* var. *neoformans* and var. *grubii*, as well as *C. gattii*, strains (Fig. 1A). Comparison of All1p and All2p amino acid sequences revealed that they are highly homologous (77% similarity and 61% identity) (Fig. 1B). Homology in the N-terminal part of the protein (176 amino acids [aa]) was 85%, whereas homology in the C-terminal part was only 35% (58 aa). Extensive searches for putative conserved domains or protein motifs using standard motif search programs detected no conserved domains or motifs. Both All1p and All2p exhibit homology (33 to 38%) only with hypothetical proteins in *Malassezia* sp. and other nonencapsulated plant-pathogenic fungi, such as *Sterenum hirsutum* and *Rhodosporidium toruloides*. No homology with proteins of any human-pathogenic fungi was found (see Fig. S1 in the supplemental material). The *all2*Δ null mutant was generated in the *C. neoformans* RC2 (serotype D) strain by replacing the coding region of *ALL2* (RC2, 926 bp) with a neomycin resistance marker (*NEO*) of 2,098 bp using biolistic transformation. Successful homologous recombination was confirmed by PCR (see Fig. S2 in the supplemental material) and real-time PCR (see Table S3 in the supplemental material). The double mutant strain (*all1*Δ *all2*Δ) was also generated in RC2 using the previously generated *all1*Δ mutant strain (7) as the background strain.

Characterization of disruption mutants. Phenotypic characteristics of the null *all2*Δ mutant, the *all1*Δ *all2*Δ double mutant, and the reconstituted *all2*Δ+P_{ACT1}-*ALL2* strain are summarized in Table 1. Baseline capsule size and capsule induction were not affected by loss of *ALL2* either *in vitro* or *in vivo*. Measurement of the biophysical properties of shed exo-PS demonstrated that exo-PS from the RC2-*all2*Δ mutant was less viscous than exo-PS from the RC2-wt and the reconstituted strain (Fig. 2A). To quantify shed exo-PS, a phenol-sulfuric colorimetric assay, which quantifies glucuronic acid residues, was used. This experiment showed that RC2-*all2*Δ cells shed more exo-PS per cell than the wild type (Table 1). Furthermore, RC2-*all2*Δ cells have no growth defect at neutral pH and display normal melanin production. Mutant cells exhibit comparable sensitivity to lysing enzyme and various high salt concentrations (data not shown). However, *all2*Δ mutant cells exhibit increased sensitivity to oxidative stress. In the presence of hydrogen peroxide (H_2O_2), RC2-*all2*Δ cells demonstrated a larger zone of inhibition in disc diffusion assays than the wild-type cells (65 versus 57 mm). This defect was resolved with gene reconstitution in RC2-*all2*Δ+P_{ACT1}-*ALL2* (58 mm) (Table 1). Consistent with this finding, incubation of mutant cells (*all2*Δ and *all1*Δ *all2*Δ) with 5 mM H_2O_2 for 3 h resulted in significantly enhanced killing ($P < 0.001$) compared to that seen with the wild type and the reconstituted strain (Fig. 2B and C). Macrophage-mediated killing assays showed significantly enhanced ($P < 0.001$) killing of RC2-*all2*Δ cells compared to cells of the wild type and the reconstituted strains (Fig. 2D). Further, antibody-mediated phagocytosis was enhanced ($P = 0.042$) for the *all2*Δ mutant (Fig. 2E). Notably, an *all2*Δ mutation was also generated in the standard laboratory strain H99, a serotype A strain and also a clinical isolate. The phenotype of the mutant in H99 was similar with respect to viscosity and H_2O_2 sensitivity but not macrophage-mediated phagocytosis (see Table S4 in the supplemental material).

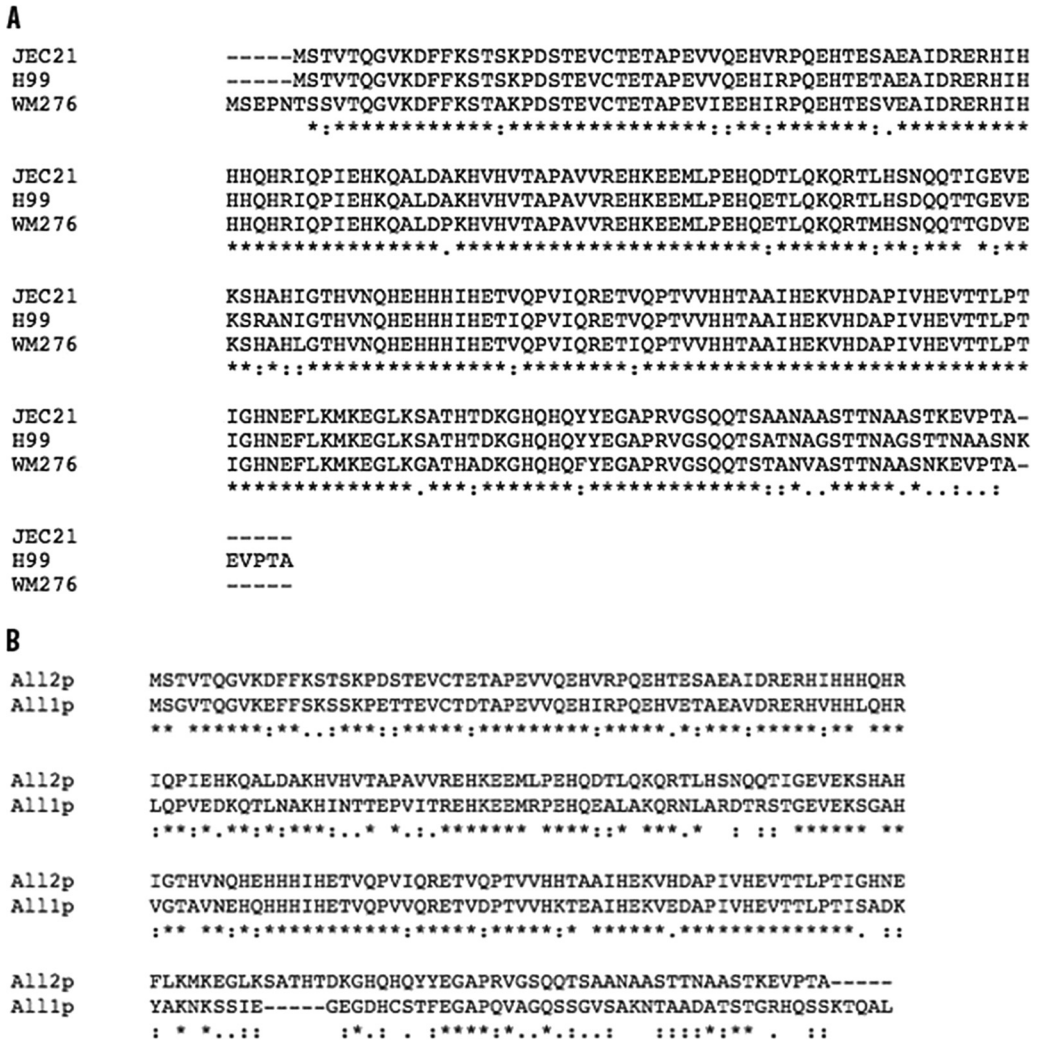

FIG 1 (A) *ALL2* is conserved among *C. neoformans* var. *neoformans*, *C. neoformans* var. *grubii*, *and C. gattii* strains. (B) Homology blast of All1 and All2 protein sequences. All2p has a 77% similarity and a 61% identity to All1p.

Loss of *ALL2* results in attenuated virulence in pulmonary cryptococcosis but not in CME. Next, virulence of *all2*Δ mutants in pulmonary and i.v. murine infection models was compared to that of wild-type and reconstituted strains. Mice infected i.t. with an inoculum of 5×10^4 RC2-*all2*Δ cells survived significantly longer ($P < 0.001$) than those infected with the wild-type strain (Fig. 3A), which was consistent with the enhanced macrophage-mediated killing and phagocytosis observed *in vitro* (Fig. 2D and E). Consistent with the unaltered growth of the mutants, comparable fungal burden was detected in the lung at 7 days postinfection, but then decreased CFU levels were found at 14 days postinfection in the mutant cells (log 5.3 ± 1.9, 3.1 ± 0.6, and 4.9 ± 1.3 for RC2-, RC2-*all2*Δ-, and RC2-*all2*Δ+P_{ACT1}-*ALL2*-infected mice, respectively, $P <$ 0.05) (Fig. 3B), which is consistent with their enhanced clearance from the lungs. In contrast, virulence in the i.v. infection model for the *all2*Δ strain was comparable to that for the wild-type and the reconstituted strains (Fig. 3C). The *all1*Δ *all2*Δ double mutant was hypovirulent in both infection models (Fig. 3D).

Histopathology analysis of RC2-*all2*Δ-infected lung tissues at 14 days revealed decreased numbers of cryptococcal cells and pronounced recruitment of inflammatory cells in the lung tissue compared to results for the wild-type-infected lung tissues (Fig. 3E). This is consistent with a more effective host response, which results in enhanced clearance and thus explains the lower fungal burden at day 14. In summary, these findings confirm that *ALL2* is a virulence-associated gene and that its loss can alter the pathogenesis of pulmonary cryptococcal infection.

The *ALL2*-fluorescent fusion protein localizes to the cytoplasm and vacuoles. Next, we sought to investigate whether All1p and All2p proteins colocalize, since both the *ALL1* and the *ALL2* transcripts are coregulated (9). For these studies, *ALL2* was fused with *C. neoformans* codon-optimized mCherry under an *ACT1* promoter (*ALL2*-mCherry). The *ALL2*-mCherry was transformed in cells expressing *ALL1* with a hemagglutinin (HA) tag under its native promoter (*ALL1*::HA). *ALL1*::HA was detected using antibodies against HA that were conjugated to Alexa Fluor 594 (green). Immunofluorescence staining revealed that All1p and All2p fusion proteins colocalize in the cytoplasm (Fig. 4A), and the protein location was found to be unaffected at multiple time points of cell growth (data not shown). However, protein expression

TABLE 1 Characteristics of the mutants[a]

Characteristic	RC2-SM	RC2-*all2*Δ	RC2-*all2*Δ+P_{ACT1}-*ALL2*	RC2-*all1*Δ*all2*Δ
Mean capsule diam (μm) ± SEM				
In vitro	1.2 ± 0.8	1.0 ± 0.4	1.3 ± 0.65	1.5 ± 0.43
In vivo	10.8 ± 2.6	11.7 ± 2.7	11.8 ± 1.5	ND
Presence of melanin	Yes	Yes	Yes	Yes
Mean growth period (h) ± SEM at:				
pH 4	2.3 ± 0.2	2.8 ± 0.1	2.8 ± 0.1	ND
pH 7	2.9 ± 0.8	2.4 ± 0.7	2.5 ± 0.6	ND
Mean phagocytosis index ± SEM	93.2 ± 16.3	113.2 ± 20.3	72 ± 8.9	109.6 ± 32.4
Zone size (mm) on:				
YNB + disc containing 5 μl of 30% H_2O_2	57	65	58	72
MM + disc containing 5 μl of 30% H_2O_2	54	62	58	64
SAB + disc containing 5 μl of 30% H_2O_2	30	40	34	38
Glucuronic acid content (mg/cell)	1.40×10^{-13}	1.57×10^{-12}	5.32×10^{-14}	ND

[a] SM, smooth; SEM, standard error of the mean; MM, minimal medium; SAB, Sabouraud broth; ND, not determined.

varied widely among yeast cells, and a majority of *C. neoformans* cells expressed only either All1p or All2p (82%). Phase-contrast microscopy indicated that the All2-mCherry fusion protein also localized to the yeast vacuoles (Fig. 4B). This finding was confirmed by vacuole-specific BCECF-AM staining of yeast cells. Variable pH and glucose did not alter the amount of All2p accumulation in vacuoles. Further, cells recovered from the lungs and the brains of mice 9 days postinfection displayed All2p localization in vacuoles (see Fig. S3 in the supplemental material).

***ALL2* is highly expressed under stress conditions, and its loss affects the expression of genes involved in multiple pathways of transport.** Review of published transcriptional profiles of *Sp1*Δ under glucose starvation documented upregulation of *ALL2* in addition to *ALL1* (9). Quantification of *ALL2* expression by RT-PCR in cells grown for 3 h in asparagine stress media and then transferred to yeast nitrogen base media under glucose (Fig. 5A) or asparagine (Fig. 5B) starvation confirmed elevated expression of *ALL2* in both stress conditions. Comparison of transcriptomes from RC2-*all2*Δ and RC2-wt cells grown in minimal media documented downregulation of 20 genes and upregulation of 263 genes in RC2-*all2*Δ cells (Table 2; see also Fig. S4 in the supplemental material). Downregulated genes included a hypothetical protein involved in carbohydrate transport and metabolism (CNE05330, 7.6-fold), a D-galactonate transporter (CNE05340, 4.1-fold), and a cluster of proteins that have in common a domain for 5-oxoprolinase (CNE05320, 2.1-fold; CNE05310, 2.5-fold). The 5-oxoprolinase (EC 3.5.2.9) enzyme is ATP dependent and is involved in glutathione metabolism to synthesize L-glutamate from 5-oxoproline.

Interestingly, the most abundant upregulated gene was a plasma membrane H^+-ATPase 1 (CNN01260, 9-fold). Other genes upregulated in the mutant were involved in multiple amino acid biosynthesis pathways: aminoacyl-tRNA biosynthesis (CNF00070, CND06300, CNM01290, CNG01310, and CNB05640), valine, leucine, and isoleucine biosynthesis (CNA02070), and purine (CNK02180, CNN00440), glutamate (CNJ02910), and glutathione (CNN00350 and CNG01150) metabolism (Table 2). Differential expression of the plasma membrane H^+-ATPase (CNN01260) and other highly regulated genes was further confirmed by RT-PCR (Fig. 5C). Importantly, the loss of *ALL2* or *ALL1* did not result in increased expression of the respective homologous genes. Transcriptomes of *all1*Δ *all2*Δ and *all1*Δ mutants grown in minimal media were also compared with that of the *all2*Δ mutant. An overlap of genes was noted only with *all1*Δ *all2*Δ cells but not with *all1*Δ cells (GEO accession number GSE74219). This further supported our conclusion that *ALL1* and *ALL2* have distinct functions.

Lastly, gene ontology (GO) analysis of differentially expressed genes in the *all2*Δ mutant under starvation conditions was consistent with the above findings. This analysis identified specific GO categories, namely, those related to transport, nucleotide binding, transmembrane transport, and catalytic activity among others (Table 3).

Intracellular pH, ATP levels, and chronological aging are altered in the *all2*Δ mutant. The main intracellular pH (pH_i) regulator in all eukaryotic cells is the plasma membrane H^+-ATPase pump (27). To measure vacuolar pH, yeast cells were stained with a pH-sensitive fluorophore, BCECF-AM. Vacuole-specific labeling was confirmed by microscopy (Fig. 6A), and calibration curves were generated (Fig. 6B) using the ratio of fluorescence intensity from excitation at 450 to 490 nm (both measured at an emission wavelength of 535 nm) at variable pHs. We measured pH_i of yeast cells grown in YNB supplemented with 2 or 0.2% glucose at medium pH 4 or 7. The pH_i were comparable in cells grown at pH 7 under both conditions (Fig. 6C). However, in cells grown at an acidic pH, the mutant was not capable of maintaining intracellular pH compared to the wild type and the reconstituted strains. As a result, the pH_i of RC2-*all2*Δ was significantly more acidic than that of the wild type (Fig. 6D). Next, we investigated the actual function of the plasma membrane H^+-ATPase 1 (CNN01260) in the *all2*Δ mutant under different pH conditions. The primary function of ATP synthase in most organisms is ATP synthesis (28). This enzyme is part of complex V ATP synthase in the oxidative phosphorylation pathway in *C. neoformans*. Accordingly, we quantified ATP cellular levels in RC2-*all2*Δ cells using an ATP bioluminescence assay kit (Sigma-Aldrich, St. Louis,

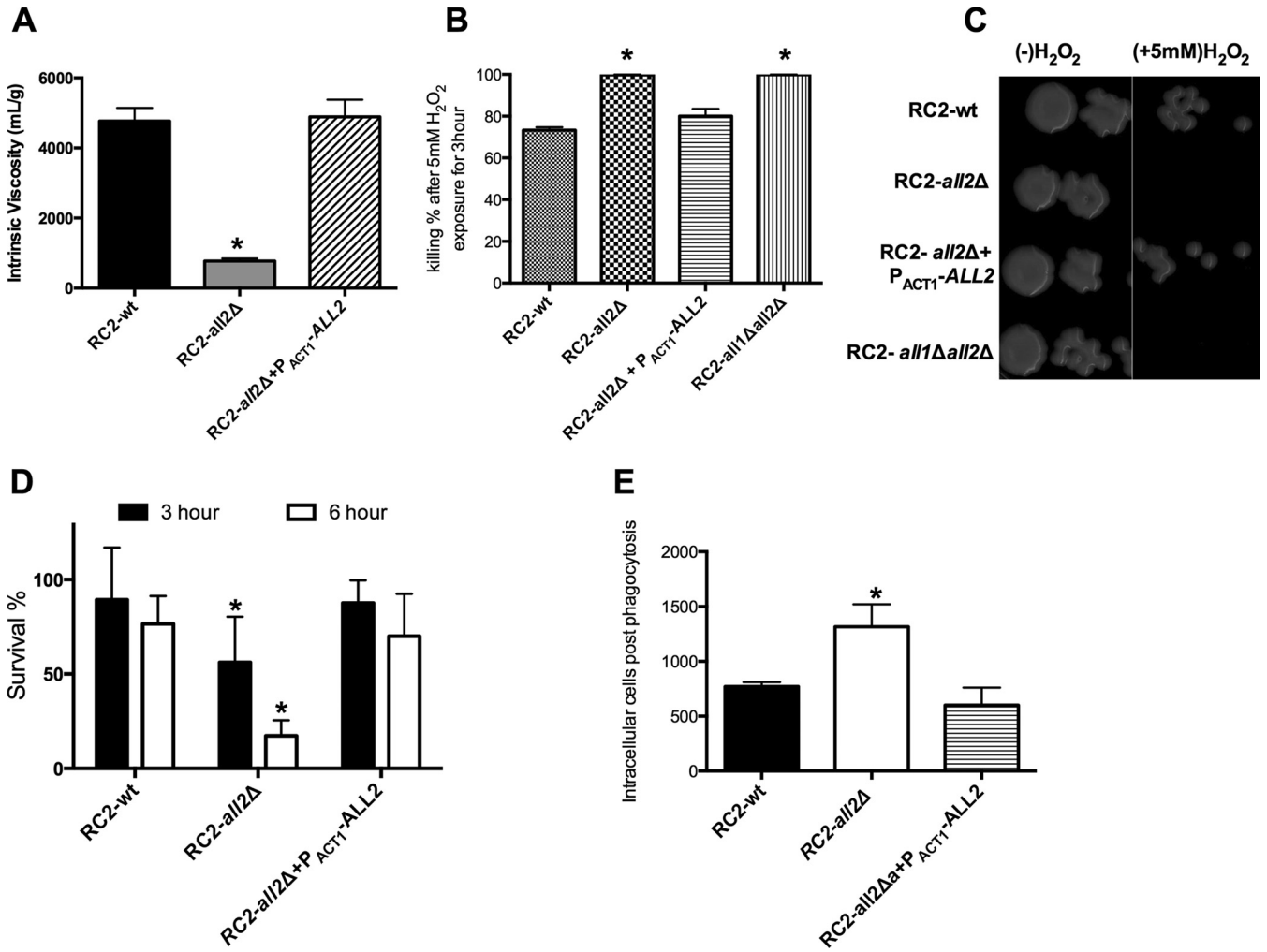

FIG 2 (A) Viscosity measurements of the exopolysaccharide shed from wild-type (RC2-wt), mutant (RC2-*all2*Δ), and reconstituted (RC2-*all2*Δ+P_{ACT1}-*ALL2*) strains grown for 14 days in minimal medium. Shed capsular polysaccharide of the *all2*Δ mutant was less viscous. The *all2*Δ mutant had increased sensitivity to H_2O_2 *in vitro*, as documented by incubating 10^5 or 10^6 RC2-wt, RC2-*all2*Δ, and RC2-*all2*Δ+P_{ACT1}-*ALL2* cells in DMEM with 5 mM H_2O_2 for 3 h and quantification of the percent survival (B) and by spotting 5 μl on YPD agar (C). (D) Killing assays were performed by lysing murine macrophages 3 h or 6 h after coincubation and plating the CFU. *all2*Δ cells were more sensitive to macrophage killing, consistent with their increased sensitivity to H_2O_2 *in vitro*. (E) The phagocytosis index determined at 2 h after coincubation was significantly higher in macrophages incubated with RC2-*all2*Δ cells than in macrophages coincubated with RC2-wt or RC2-*all2*Δ+P_{ACT1}-*ALL2* cells. Intracellular phagocytosis index was calculated by visually counting cells on a microscope. All experiments were performed in triplicates. An asterisk denotes a *P* value of ≤0.05.

MO). These experiments demonstrated that RC2-*all2*Δ cells grown in minimal media or YNB for 16 h produced significantly less cellular ATP per μg protein than the wild-type cells when grown at pH 4 (Fig. 6E) and produced comparable levels of ATP at pH 7 (Fig. 6E). Finally, chronological life span (CLS) was assessed in the mutant and compared to that in the wild type because the CLS, which is a resilience trait of yeast strains and measures their viability under no nutrition, was predicted to shorten in the setting of impaired intracellular pH regulation. Consistent with this hypothesis, we found a significantly shortened CLS in the RC2-*all2*Δ strain compared to that in the wild type (8 days versus 14 days, $P = 0.01$, Fig. 6F). It is noteworthy that the replicative life spans of the mutant and the wild type, which measures the reproductive ability as opposed to the viability of the cell, were comparable under 2% glucose and not 0.05% glucose. Under low-glucose conditions, the RC2-*all2*Δ cells had a significantly shortened RLS compared to that of the wild-type cells (21 versus 28 generations, $P = 0.02$).

DISCUSSION

In this study, we report the role of a novel virulence-associated gene named *ALL2*, which is coregulated with a highly homologous gene, *ALL1*, during the process of phenotypic switching of *C. neoformans* to a hypervirulent mucoid variant.

ALL2p is highly homologous (77% similarity and 61% identity) to the previously described gene ALL1p (7) and is also regulated by the same transcriptional regulator, Sp1 and gene *PKC1* (9), both of which are activated under stress. Our data demonstrate, however, that the functions of the two genes are mostly distinct, although both mutants exhibit enhanced exopolysaccharide secretion. The effects of gene loss on virulence and exo-PS viscosity are contrasting. It is conceivable that these two genes may

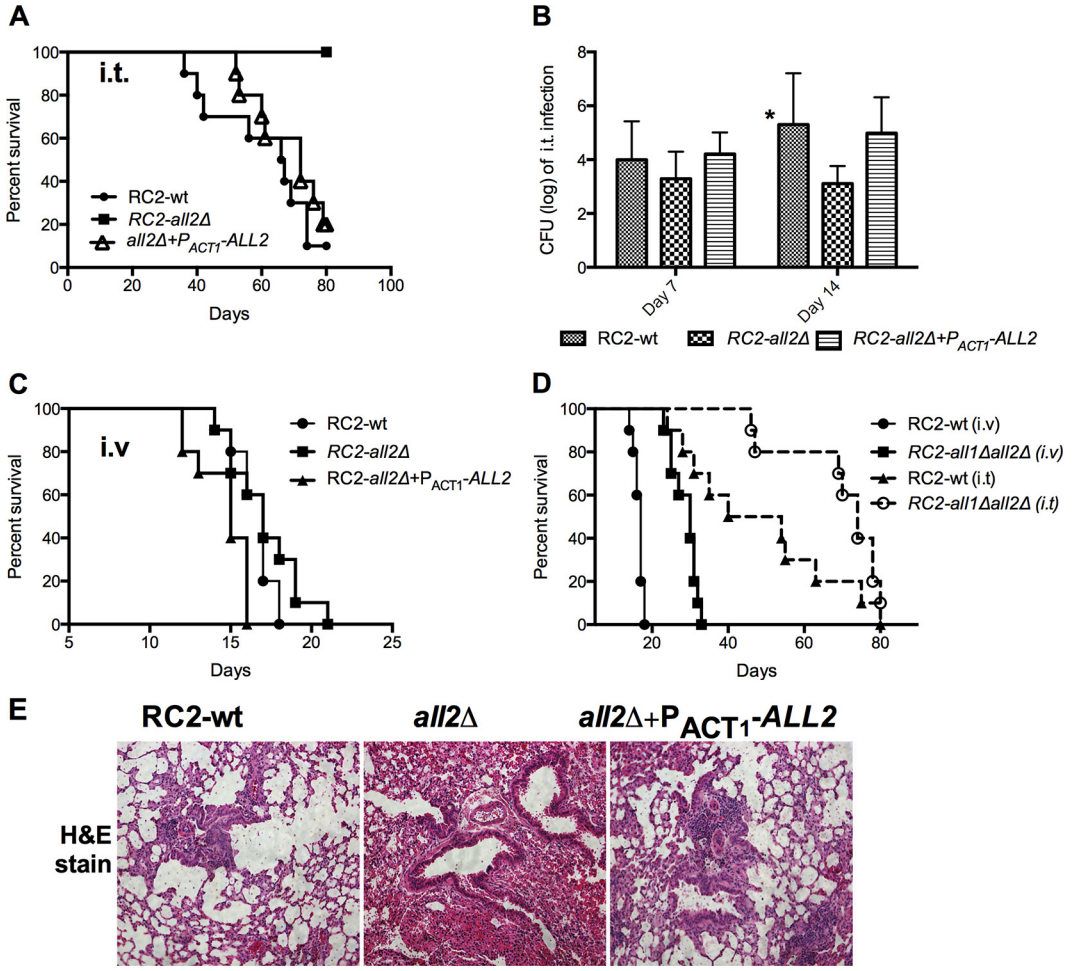

FIG 3 RC2-*all2*Δ mutants have attenuated virulence in a murine pulmonary infection model. (A) Mice infected i.t. with the mutant strain survived significantly longer than those infected with the wild-type or reconstituted strain ($P = 0.0002$). (B) Mice infected with 5×10^4 cells i.t. had comparable lung fungal burdens of log 3.9 ± 1.4, 3.2 ± 1.2, and 4.1 ± 0.8 for RC2-wt, RC2-*all2*Δ, and RC2-*all2*Δ+P$_{ACT1}$-*ALL2* strain-infected mice, respectively, at 7 days postinfection. However, consistent with the survival difference, RC2-*all2*Δ strains had a lower lung fungal burden at 14 days postinfection (log 5.3 ± 1.9, 3.1 ± 0.6, and 4.9 ± 1.3 for wild-type, *all2*Δ, and *all2*Δ+P$_{ACT1}$-*ALL2* strain-infected mice, respectively [$P = 0.04$]). (C) No difference in survival was noted in an i.v. infection model between the wild-type and RC2-*all2*Δ mutant strains. (D) The double mutant (RC2-*all1*Δ*all2*Δ) was hypovirulent in both the i.t. and i.v. models. (E) Histopathology of lungs stained with hematoxylin and eosin (H&E) and infected with 10^4 cells was examined. On day 14, lung histology revealed that RC2-*all2*Δ-infected mice had a more pronounced host response, resulting in enhanced clearance of lung fungal burden compared to wild-type- and reconstituted strain-infected mice. Lower numbers of yeast cells and more inflammatory cells were observed in the alveolar spaces of RC2-*all2*Δ infected mice than for wild-type- and RC2-*all2*Δ+P$_{ACT1}$-*ALL2*-infected mice. An asterisk denotes a *P* value of ≤0.05.

be paralogs, or duplicated genes that over time have come to be different in sequence composition and function.

Loss of *ALL1* leads to hypervirulence and early death, whereas the loss of *ALL2* leads to hypovirulence and prolonged survival. Interestingly, hypovirulence is observed in the pulmonary infection model only and not in the i.v. infection model. In the latter model, dissemination across the blood-brain barrier occurs immediately, whereas in the i.t. model, fungal infection is initially controlled by alveolar macrophages, and dissemination to the brain occurs secondarily, usually after 1 to 2 weeks. Mice infected with *all2*Δ cells eventually exhibited lower CFU in lung tissue, consistent with their impaired resilience in the host environment. Similar results were demonstrated in mice infected with *all1*Δ *all2*Δ yeast cells, which also lived longer, albeit their mortality was more rapid. This was not expected from partial suppression of *all2*Δ by *all1*Δ since their expression levels remain unchanged based on the microarray data.

C. neoformans is a facultative intracellular pathogen (29, 30) that has developed mechanisms to counteract the stress it encounters inside macrophages. Experiments in murine infection models suggest that the outcome of cryptococcal infection correlates with the ability of alveolar macrophages to control intracellular fungal replication (30–32). A higher budding index for intracellularly located than for extracellularly located *C. neoformans* has been described in murine pulmonary infection (29), supporting the notion that this niche is important in pathogenesis, as it permits fungal growth. Also, murine alveolar macrophages appear to have less killing efficacy than rat macrophages and therefore support enhanced intracellular replication (32). Recent experiments support the concept that human and murine macrophages exhibit comparable efficacies with respect to supporting *C. neoformans* growth (33). Furthermore, two independent investigations with clinical *C. neoformans* strains derived from different patient cohorts with CME, although their conclusions differed slightly, sup-

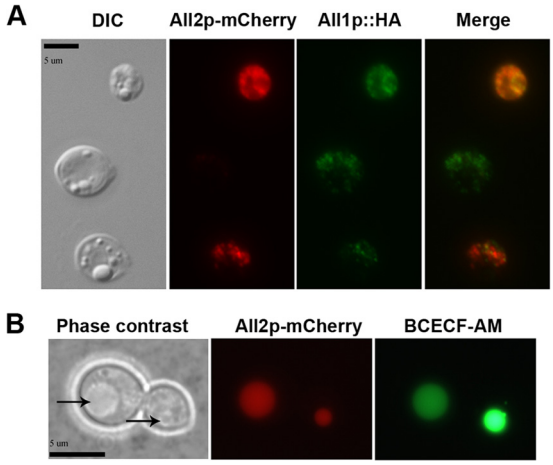

FIG 4 (A) All2p-mCherry fusion proteins localize in the cytoplasm, with accumulation in vacuoles. For coexpression studies, single cells expressing All2p-mCherry (red) and All1p::HA (green) fusion proteins were grown in YNB for 16 h at 37°C and observed by using differential interference contrast microscopy and fluorescence. The imaging revealed the cytoplasmic location and colocalization of both fusion proteins. (B) All1-mCherry fusion proteins were also found to colocalize in yeast vacuoles by phase-contrast microscopy (indicated by an arrow) and BCECF-AM staining (scale bar, 5 μm).

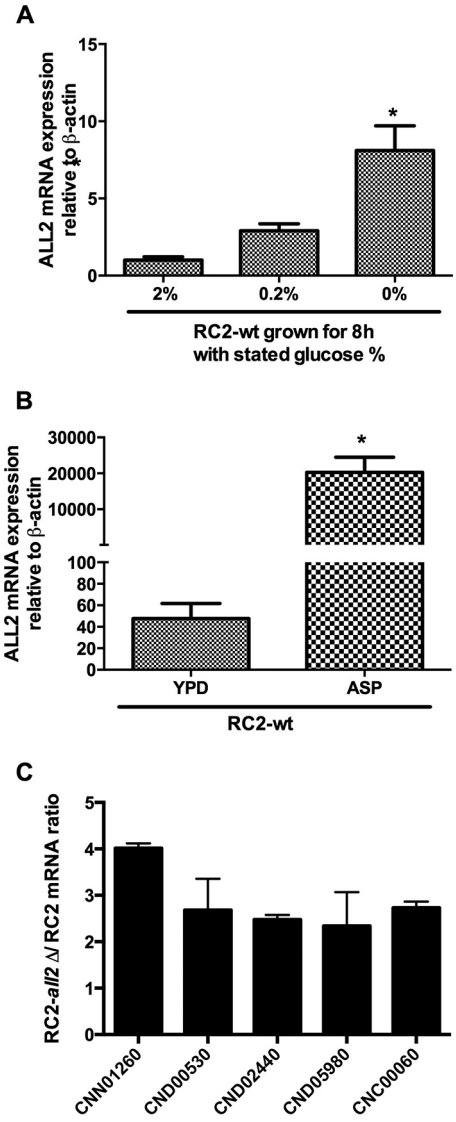

FIG 5 *ALL2* transcription was highly induced under glucose starvation (A) and in asparagine stress medium (B). The transcription of *ALL2* was measured by RT-PCR in RNA obtained from cells incubated in YNB without glucose and in YNB with 0.2 or 2% glucose for 8 h, as well as from cells incubated in asparagine medium without glucose for 3 h at 37°C. The *ACT1* gene was used as a control. (C) RT-PCR analysis confirmed the microarray results showing the upregulation of transport-related genes in RC2-*all2*Δ cells, including H^+-ATPase (CNN01260).

port the notion that growth of the yeast in the intracellular niche affects evasion of the immune response and nonsterilization of CSF (33, 34). Our data now indicate that the function of All2p contributes through diverse mechanisms to reduce the efficacy of this key immune cell.

Similarly to the antimicrobial activity against other microorganisms, reactive oxygen species are key mediators of the anticryptococcal activity of macrophages and neutrophils (35–39). Iron catalyzes the generation of hydroxyl radicals from oxidant precursors, such as superoxide anions and hydrogen peroxide (40). Gene ontology analysis of differentially expressed genes has shown that adaptation of *C. neoformans* to H_2O_2 treatment is distinct from the response of other fungal organisms to oxidative stress (41). One reason for this is that *C. neoformans* is encapsulated and both the size and the biophysical properties of the exo-PS of *C. neoformans* affect its resistance to oxidative stress (13, 17). Our results now demonstrate that the exo-PS of *all2*Δ cells is augmented and has altered biophysical properties, namely, decreased viscosity compared to the exo-PS of the wild type. In contrast to this, the loss of *ALL1* resulted in the secretion of a hyperviscous exo-PS and manifestation of a hypervirulent phenotype in murine models (12). The *ALL2* mutant exhibits no significant growth defects in rich or nutrient-limiting media. Hence, we propose that the hypovirulence observed in pulmonary, but not in i.v., infection stems from an altered resistance to host response and from pH rather than nutrient differences in the two infection sites. The inability of *all2*Δ cells to buffer the low pH inside alveolar macrophages likely contributes to the loss of yeast cell viability in the intracellular niche. A slightly slower growth at lower pH supports this concept.

Although both *ALL1* and *ALL2* transcripts are expressed during logarithmic growth *in vitro* (9), they achieve maximal expression under starvation in the stationary growth phase. Localization studies with labeled protein constructs revealed some colocalization of All2p with All1p in the cytoplasm, although they did not accumulate in vacuoles as described for the membrane transporter *CTR1* (42) and the copper transporter *CTR4* (21). It appears that mCherry has a tendency to accumulate in vacuoles after degradation (21), and our interpretation is that vacuolar localization of All2p is not specific. This could indicate that All2p undergoes a significant level of degradation as previously reported for H^+-ATPase in *S. cerevisiae* (43) and ctr4-ctr5 in *Schizosaccharomyces pombe* (44). Despite coexpression and, most importantly, coregulation by the same transcription factors, our data suggest distinct functions of *ALL2* and *ALL1* except for the fact that both mutants exhibit augmented exo-PS shedding. Also, respective GO analysis of the mutants identified regulated genes in the transmembrane transport category. In support of these conclusions, no

TABLE 2 *ALL2* in acidic growth conditions regulates genes involved in transport and multiple pathways

GO function and *C. neoformans* gene	Description	Fold change (mutant/wt)
Transport		
CND02440	Peptide transporter	4.30
CND00530	Urea transporter	3.70
CND05980	Nucleoside transporter	3.40
CNA07090	ABC transporter	2.60
CNE00270	Amino acid transmembrane transporter	2.57
CNA05800	Amino acid transporter	2.43
CNB02200	RAN protein binding protein	2.27
CNC05860	Metal resistance protein	2.10
Nucleotide binding		
CNN01260	Plasma membrane H^+-ATPase 1	9.50
CNL04860	ATPase activity	2.70
CND06300	Aspartate-tRNA ligase	2.23
CNG01310	Arginine-tRNA ligase	2.23
CNB05640	Proline-tRNA ligase	2.21
CNF00070	Glutamate-tRNA ligase	2.02
CNK00560	DNA polymerase	2.08
CNM01290	Leucine-tRNA ligase	2.05
CNN00350	Glutamate-cysteine ligase	2.03
Transmembrane transport		
CNC00060	Sugar transporter	3.07
CND05980	Folic acid metabolism	2.92
CND04690	Sugar transporter	2.90
CNI03510	Allanote transmembrane transporter	2.88
CNH01210	Phosphate transmembrane transporter	2.73
CNC04510	Siderophore (ion) uptake	2.71
CNG04630	Efflux protein EncT	2.64
CNJ01450	Multidrug transporter activity	2.58
CNE01880	Pantothenate transporter	2.57
CNF01220	Allantoate transmembrane transporter	2.30
CNF00350	Hypothetical protein	2.08
CNG01480	Fructose transmembrane transporter	2.08
CNC03220	Receptor glucose binding	2.07
CNI03490	Sugar transporter	2.03
CNC01890	Na^+/H^+ exchange	2.00
CNE05340	Allantoate membrane transporter	−4.01
Catalytic activity		
CNA02570	Acetolactate synthase	3.46
CNG00590	Folic acid metabolism	2.92
CNC00360	Protein phosphatase	2.83
CNG01150	Spermidine synthase	2.78
CNE00720	Hypothetical protein	2.46
CNG04420	α-1,3-Glucan synthase	2.34
CNN00440	Purine nucleotide biosynthesis	2.33
CNA07740	Acetate coligase	2.28
CNI03300	Phosphoribosylformylglycinamidine synthase activity	2.05
CNB03190	Hypothetical protein	2.01
CNE05320	5-Oxoprolinase	−2.10
Glucogenesis		
CNI03590	Phosphoenolpyruvate carboxykinase, putative	3.02
CNJ00950	Pyruvate decarboxylase	2.35
CNB04050	Glucose 6-phosphate isomerase	2.20
Protein binding		
CNG00480	Atomer alpha subunit	3.64
CNG02370	tRNA (guanine) methyltransferase	3.28
CNC02150	Translation initiation factor	2.92

(Continued on following page)

TABLE 2 (Continued)

GO function and *C. neoformans* gene	Description	Fold change (mutant/wt)
CNJ02300	Structural molecule activity	2.77
CNH02560	Hypothetical protein	2.70
CNG02820	Protein phosphate regulator	2.69
CNE01020	Translation initiation factor	2.68
CNB00260	Hypothetical protein	2.59
CNN01950	Hypothetical protein	2.41
CNJ01250	Hypothetical protein	2.39
CNA04270	HMG1 chromatin binding	2.38
CNA04050	Elongation factor	2.35
CNK01990	Hypothetical protein	2.25
CNB05570	ER-to-Golgi body transport	2.22
CNJ00610	Argonaute-like protein	2.13
CNJ00830	Hypothetical protein	2.13
CNL05140	Hypothetical protein	2.13
CNA04910	Retrograde transport; endosome to Golgi body	2.13
CNB04960	Hypothetical protein	2.10
CNK02410	General transcription repressor	2.10
CNE03290	Translation initiation factor	2.10
CNA00630	Nuclear mRNA splicing	2.07
CNA06050	Guanyl-nucleotide exchange factor	2.01
RNA binding		
CNI01160	Poly(A) binding	4.01
CNA01020	Pre-mRNA splicing factor activity	2.00
CNE01200	rRNA processing-related protein	3.11
CNC04280	mRNA binding	2.89
CNE05380	RNA-directed DNA polymerase activity	2.10
CNH03600	Pseudouridine synthase	2.35
CNJ03440	RNA-directed DNA polymerase activity	−2.04
CNF04940	RNA-directed DNA polymerase activity	−2.17

change in the expression levels in either mutant to compensate for the loss of the other gene was observed. Also, efforts to coprecipitate the two proteins were not successful (data not shown).

Transcriptome comparison of *all2*Δ and wild-type cells revealed differential expression of multiple transporters and nucleotide binding proteins, with significant downregulation of 5-oxoprolinase and the highest upregulation of a plasma membrane, H^+-ATPase. 5-Oxoprolinase is an enzyme involved in the gamma-glutamyl cycle for glutathione metabolism and catalyzes the cleavage of 5-oxoproline to form L-glutamate in a reaction coupled to the hydrolysis of ATP to ADP and inorganic phosphate (28). Glutathione metabolism is crucial for amino acid transport *in vitro*, as well as *in vivo* (45); however, in *S. cerevisiae*, deletion of 5-oxoprolinase results in the accumulation of 5-oxoproline (46). The protein localizes to the cytoplasm and an abundant increase in response to stress is observed.

TABLE 3 GO terms identified in the differentially expressed genes

GO term	Description	*P*	
		Hypergeometric test	Bonferroni's test
GO:0006810	Transport	2.2×10^{-5}	4.2×10^{-3}
GO:0000166	Nucleotide binding	3.79×10^{-5}	7.0×10^{-3}
GO:0055085	Transmembrane transport	4.16×10^{-4}	7.7×10^{-3}
GO:0005215	Transporter activity	5.61×10^{-4}	7.8×10^{-2}
GO:0003824	Catalytic activity	7.96×10^{-4}	0.104
GO:0006094	Glucogenesis	8.06×10^{-4}	0.15
GO:0005515	Protein binding	1.57×10^{-3}	0.29
GO:0005524	ATP binding	1.69×10^{-3}	0.31
GO:0003723	RNA binding	1.87×10^{-3}	0.34

Plasma membrane H^+-ATPase, CNM01260, encodes a protein that has a high homology to an isoform of Pma1p, a plasma membrane H^+-ATPase that is involved in pumping protons out of the cell. This enzyme is a regulator of intracellular pH and maintains the electrochemical proton gradient necessary for nutrient uptake. GO analysis indicates that this gene is associated with several processes, including ATP catabolic and biosynthesis process, cation transport, nucleotide binding, ATP binding, hydrolase activity, and ATPase activity. The gene is an integral component of the plasma membrane (http://www.ebi.ac.uk/QuickGO/GProtein?ac=F5HCX1).

Mutations in *PMA1* that encode H^+-ATPase of *S. cerevisiae* lead to decreased levels of ATPase, which has been correlated with decreased proton efflux and decreased uptake of amino acids (47). How exactly All2p and Pma1 interact remains to be determined. Our data indicate that upregulation of H^+-ATPase gene expression in the *all2*Δ mutant does not compensate for the loss of *PMA1* because the mutant still exhibited low ATP production and was inefficient in maintaining intracellular pH in acidic conditions. Maintaining intracellular pH is crucial under starvation conditions in the phagosome because, in contrast to *Candida albicans* and *Candida glabrata* (48, 49), *C. neoformans* does not interfere with phagosome maturation. Thus, the *C. neoformans* containing

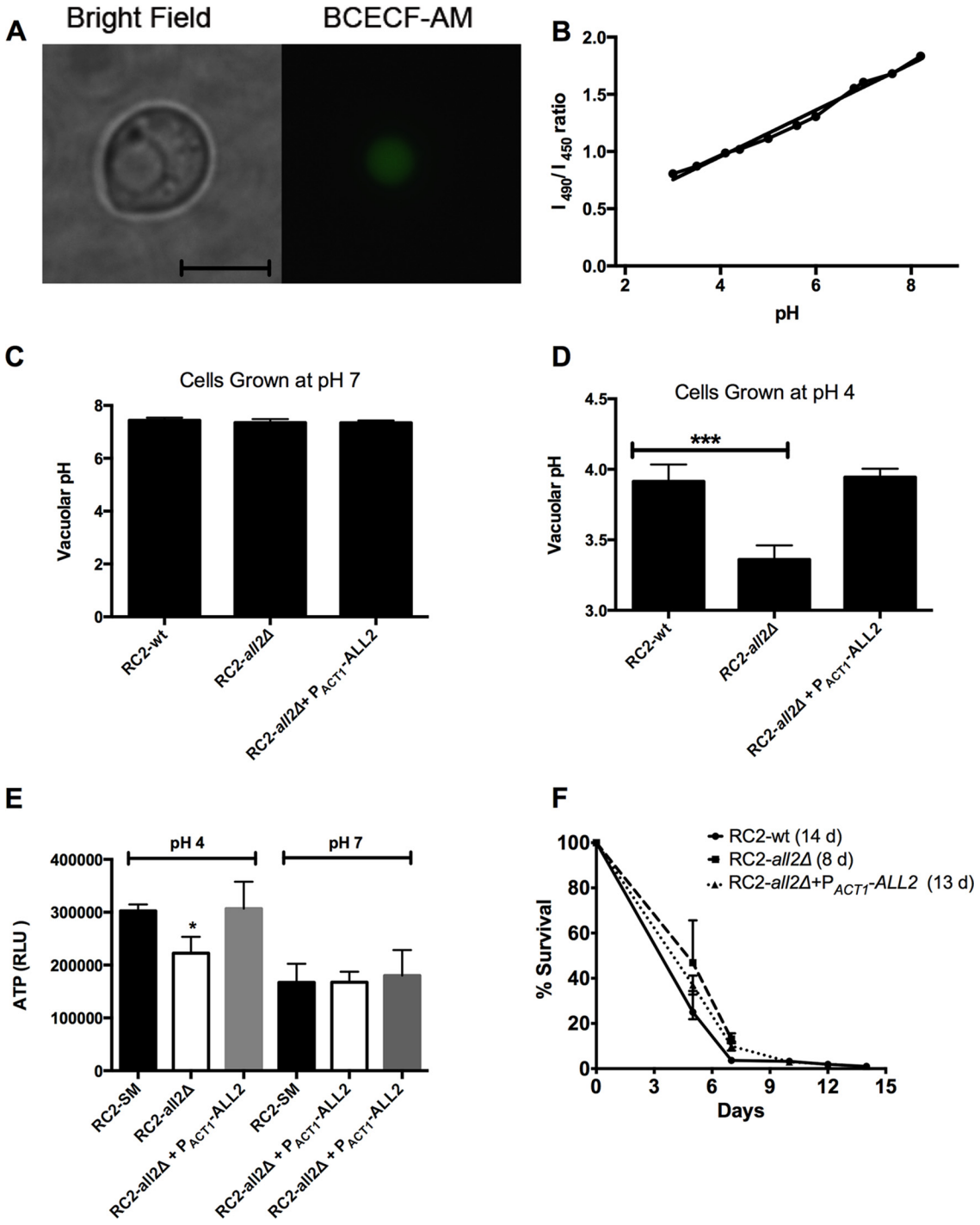

FIG 6 Intracellular pH measurement of *C. neoformans* RC2-wt and RC2-*all2*Δ cells. (A) BCECF-AM successfully stained vacuoles of *C. neoformans* (scale bar, 5 μm). (B) Calibration curves were generated using ratio of fluorescence intensity from excitation at 450 to 490 nm (both measured at an emission wavelength of 535 nm) at varied pH. The pH_i were comparable in cells grown at pH 7 (C) and found to be significantly different between RC2-wt and RC2-*all2*Δ cells when grown in acidic pH conditions (D). (E) RC2-*all2*Δ mutant cells exhibited significantly less ATP production per μg of protein than RC2-wt cells at pH 4 but comparable levels at pH 7. (F) The CLS of RC2-wt cells was significantly longer than the CLS of *all2*Δ cells (14 versus 8 days, $P < 0.001$), as measured by survival in water. An asterisk denotes a *P* value of ≤0.05.

phagosome undergoes acidification through fusion with lysosomes, and *C. neoformans* needs to buffer pH to grow inside the mature acidic vacuole (50, 51). Of note is that although *PMA1* is abundant among fungi, All2p has homologues only in basidiomycetes that prefer plants as their host.

Interestingly, no significant regulation of *ALL2* was observed in *C. neoformans* currently implicated in pH homeostasis. For instance, Rim101 is a conserved pH-responsive transcription factor that allows the microorganism to respond to pH changes (16). However, neither All2 nor Rim101 appears to be significantly reg-

ulated by the other in respective transcriptome studies (16). In a more recent study, Rim101 was shown to share downstream targets with Pka1, and not surprisingly, *ALL2* was found to be upregulated in the *pka1*Δ mutant (52). Impaired ability to maintain proper intracellular pH also explains the significantly shortened chronological life span of the mutants compared to that of the wild type. In *S. cerevisiae*, chronological aging has been shown to result in an acidic intracellular environment (25), and the inability of the mutants to neutralize pH results in a shortened chronological life span but has no effect on the replicative life span. *C. neoformans* is acquired by inhaling spores from the environment. Most clinical manifestations of infections represent reactivation of latent disease (53). The intracellular environment of macrophages in small granulomas is likely the site where the fungus survives nonreplicating for decades, similar to the pathogenesis of latent tuberculosis. Chronological aging is a distinct trait of resilience as it measures the ability of a fungus to survive in a nonreplicating state. Although this trait has not been studied with respect to pathogenesis, we propose that this form of resilience is critical for the establishment of latency of cryptococcal infection.

It has been reported previously that the overexpression of H^+-ATPase is compensated by the downregulation of H^+-ATPase activity *in vivo* (54) and does not always enhance growth (55). In *S. cerevisiae*, *PTK2* and *HRK1* genes encode protein kinases that have been identified to activate yeast plasma membrane production in response to glucose activation (56). Of note, *ALL1* and *ALL2* are regulated by the protein kinase Pkc1 signaling pathway (9). In contrast to the plasma membrane H^+-ATPase of *S. cerevisiae*, which is upregulated by glucose (57), *ALL1* and *ALL2* are upregulated in the setting of low glucose levels.

In summary, we conclude that the attenuated virulence of the *all2*Δ mutant in the pulmonary infection model may result from the mutant's inefficiency to maintain intracellular pH in an acidic phagosome environment. The *all2*Δ mutant has no dramatic growth defect but produces significantly lower levels of ATP than the wild type, which affect the energetic state of the *all2*Δ mutant *in vivo*. We reason that this changes its resilience and the outcome of infection, similarly to *Leishmania donovani*, where intracellular ATP levels correlate with parasite proliferation (58).

We propose that *ALL2* should be considered a target for antifungal drug discovery and further studied. Our studies highlight the uniqueness of *C. neoformans*, one of the few basidiomycetes that have evolved to be a successful human fungal pathogen. Specifically, these data show that its unique ability to escape host response and survive in the intracellular niche relies on genes, such as *ALL2*, that are unique to this fungus and contribute to its exceptional resilience.

FUNDING INFORMATION

This work was supported by NIH awards R01 AI059681 and R21 A1087564 to B.C.F. The funders had no role in study design, data collection and interpretation, or the decision to submit the work for publication.

REFERENCES

1. **Park BJ, Wannemuehler KA, Marston BJ, Govender N, Pappas PG, Chiller TM.** 2009. Estimation of the current global burden of cryptococcal meningitis among persons living with HIV/AIDS. AIDS **23:**525–530. http://dx.doi.org/10.1097/QAD.0b013e328322ffac.
2. **Bicanic T, Meintjes G, Wood R, Hayes M, Rebe K, Bekker LG, Harrison T.** 2007. Fungal burden, early fungicidal activity, and outcome in cryptococcal meningitis in antiretroviral-naive or antiretroviral-experienced patients treated with amphotericin B or fluconazole. Clin Infect Dis **45:**76–80. http://dx.doi.org/10.1086/518607.
3. **Hamilton AJ, Goodley J.** 1996. Virulence factors of *Cryptococcus neoformans*. Curr Top Med Mycol **7:**19–42.
4. **Fries BC, Goldman DL, Cherniak R, Ju R, Casadevall A.** 1999. Phenotypic switching in *Cryptococcus neoformans* results in changes in cellular morphology and glucuronoxylomannan structure. Infect Immun **67:**6076–6083.
5. **Fries BC, Taborda CP, Serfass E, Casadevall A.** 2001. Phenotypic switching of *Cryptococcus neoformans* occurs in vivo and influences the outcome of infection. J Clin Invest **108:**1639–1648. http://dx.doi.org/10.1172/JCI13407.
6. **Franzot SP, Mukherjee J, Cherniak R, Chen LC, Hamdan JS, Casadevall A.** 1998. Microevolution of a standard strain of *Cryptococcus neoformans* resulting in differences in virulence and other phenotypes. Infect Immun **66:**89–97.
7. **Jain N, Li L, Hsueh YP, Guerrero A, Heitman J, Goldman DL, Fries BC.** 2009. Loss of allergen 1 confers a hypervirulent phenotype that resembles mucoid switch variants of *Cryptococcus neoformans*. Infect Immun **77:**128–140. http://dx.doi.org/10.1128/IAI.01079-08.
8. **Haynes BC, Skowyra ML, Spencer SJ, Gish SR, Williams M, Held EP, Brent MR, Doering TL.** 2011. Toward an integrated model of capsule regulation in *Cryptococcus neoformans*. PLoS Pathog **7:**e1002411. http://dx.doi.org/10.1371/journal.ppat.1002411.
9. **Adler A, Park YD, Larsen P, Nagarajan V, Wollenberg K, Qiu J, Myers TG, Williamson PR.** 2011. A novel specificity protein 1 (SP1)-like gene regulating protein kinase C-1 (Pkc1)-dependent cell wall integrity and virulence factors in *Cryptococcus neoformans*. J Biol Chem **286:**20977–20990. http://dx.doi.org/10.1074/jbc.M111.230268.
10. **Jung WH, Sham A, White R, Kronstad JW.** 2006. Iron regulation of the major virulence factors in the AIDS-associated pathogen *Cryptococcus neoformans*. PLoS Biol **4:**e410. http://dx.doi.org/10.1371/journal.pbio.0040410.
11. **Panepinto J, Liu L, Ramos J, Zhu X, Valyi-Nagy T, Eksi S, Fu J, Jaffe HA, Wickes B, Williamson PR.** 2005. The DEAD-box RNA helicase Vad1 regulates multiple virulence-associated genes in *Cryptococcus neoformans*. J Clin Invest **115:**632–641. http://dx.doi.org/10.1172/JCI200523048.
12. **Jain N, Cordero RJ, Casadevall A, Fries BC.** 2013. Allergen 1 regulates polysaccharide structure in *Cryptococcus neoformans*. Mol Microbiol **88:**713–727. http://dx.doi.org/10.1111/mmi.12216.
13. **Zaragoza O, Chrisman CJ, Castelli MV, Frases S, Cuenca-Estrella M, Rodriguez-Tudela JL, Casadevall A.** 2008. Capsule enlargement in *Cryptococcus neoformans* confers resistance to oxidative stress suggesting a mechanism for intracellular survival. Cell Microbiol **10:**2043–2057. http://dx.doi.org/10.1111/j.1462-5822.2008.01186.x.
14. **Jain N, Li L, McFadden DC, Banarjee U, Wang X, Cook E, Fries BC.** 2006. Phenotypic switching in a *Cryptococcus neoformans* variety *gattii* strain is associated with changes in virulence and promotes dissemination to the central nervous system. Infect Immun **74:**896–903. http://dx.doi.org/10.1128/IAI.74.2.896-903.2006.
15. **Mandal P, Banerjee U, Casadevall A, Nosanchuk JD.** 2005. Dual infections with pigmented and albino strains of *Cryptococcus neoformans* in patients with or without human immunodeficiency virus infection in India. J Clin Microbiol **43:**4766–4772. http://dx.doi.org/10.1128/JCM.43.9.4766-4772.2005.
16. **O'Meara TR, Norton D, Price MS, Hay C, Clements MF, Nichols CB, Alspaugh JA.** 2010. Interaction of *Cryptococcus neoformans* Rim101 and protein kinase A regulates capsule. PLoS Pathog **6:**e1000776. http://dx.doi.org/10.1371/journal.ppat.1000776.
17. **Cordero RJ, Frases S, Guimaraes AJ, Rivera J, Casadevall A.** 2011. Evidence for branching in cryptococcal capsular polysaccharides and consequences on its biological activity. Mol Microbiol **79:**1101–1117. http://dx.doi.org/10.1111/j.1365-2958.2010.07511.x.
18. **DuBois M, Gilles KA, Hamilton JK, Rebers PA, Smith F.** 1956. Colorimetric method for determination of sugars and related substances. Anal Chem **28:**350–356. http://dx.doi.org/10.1021/ac60111a017.
19. **Reilly MC, Aoki K, Wang ZA, Skowyra ML, Williams M, Tiemeyer M, Doering TL.** 2011. A xylosylphosphotransferase of *Cryptococcus neoformans* acts in protein O-glycan synthesis. J Biol Chem **286:**26888–26899. http://dx.doi.org/10.1074/jbc.M111.262162.
20. **Reilly MC, Levery SB, Castle SA, Klutts JS, Doering TL.** 2009. A novel xylosylphosphotransferase activity discovered in *Cryptococcus neofor-*

mans. J Biol Chem **284:**36118–36127. http://dx.doi.org/10.1074/jbc.M109.056226.
21. **Waterman SR, Park YD, Raja M, Qiu J, Hammoud DA, O'Halloran TV, Williamson PR.** 2012. Role of CTR4 in the virulence of *Cryptococcus neoformans*. mBio **3:**e00285-12. http://dx.doi.org/10.1128/mBio.00285-12.
22. **Plant PJ, Manolson MF, Grinstein S, Demaurex N.** 1999. Alternative mechanisms of vacuolar acidification in H^+-ATPase-deficient yeast. J Biol Chem **274:**37270–37279. http://dx.doi.org/10.1074/jbc.274.52.37270.
23. **Diakov TT, Tarsio M, Kane PM.** 2013. Measurement of vacuolar and cytosolic pH in vivo in yeast cell suspensions. J Vis Exp http://dx.doi.org/10.3791/50261.
24. **Garcia J, Shea J, Alvarez-Vasquez F, Qureshi A, Luberto C, Voit EO, Del Poeta M.** 2008. Mathematical modeling of pathogenicity of *Cryptococcus neoformans*. Mol Syst Biol **4:**183.
25. **Burtner CR, Murakami CJ, Kennedy BK, Kaeberlein M.** 2009. A molecular mechanism of chronological aging in yeast. Cell Cycle **8:**1256–1270. http://dx.doi.org/10.4161/cc.8.8.8287.
26. **Steffen KK, Kennedy BK, Kaeberlein M.** 2009. Measuring replicative life span in the budding yeast. J Vis Exp http://dx.doi.org/10.3791/1209.
27. **Serrano R.** 1988. Structure and function of proton translocating ATPase in plasma membranes of plants and fungi. Biochim Biophys Acta **947:**1–28. http://dx.doi.org/10.1016/0304-4157(88)90017-2.
28. **Alberts B, Bray D, Lewis J, Raff M, Roberts K, Watson J.** 1994. Molecular biology of the cell, 3rd ed. Taylor and Francis, New York, NY.
29. **Feldmesser M, Kress Y, Novikoff P, Casadevall A.** 2000. *Cryptococcus neoformans* is a facultative intracellular pathogen in murine pulmonary infection. Infect Immun **68:**4225–4237. http://dx.doi.org/10.1128/IAI.68.7.4225-4237.2000.
30. **Feldmesser M, Tucker S, Casadevall A.** 2001. Intracellular parasitism of macrophages by *Cryptococcus neoformans*. Trends Microbiol **9:**273–278. http://dx.doi.org/10.1016/S0966-842X(01)02035-2.
31. **Zaragoza O, Alvarez M, Telzak A, Rivera J, Casadevall A.** 2007. The relative susceptibility of mouse strains to pulmonary *Cryptococcus neoformans* infection is associated with pleiotropic differences in the immune response. Infect Immun **75:**2729–2739. http://dx.doi.org/10.1128/IAI.00094-07.
32. **Shao X, Mednick A, Alvarez M, van Rooijen N, Casadevall A, Goldman DL.** 2005. An innate immune system cell is a major determinant of species-related susceptibility differences to fungal pneumonia. J Immunol **175:**3244–3251. http://dx.doi.org/10.4049/jimmunol.175.5.3244.
33. **Sabiiti W, Robertson E, Beale MA, Johnston SA, Brouwer AE, Loyse A, Jarvis JN, Gilbert AS, Fisher MC, Harrison TS, May RC, Bicanic T.** 2014. Efficient phagocytosis and laccase activity affect the outcome of HIV-associated cryptococcosis. J Clin Invest **124:**2000–2008. http://dx.doi.org/10.1172/JCI72950.
34. **Alanio A, Desnos-Ollivier M, Dromer F.** 2011. Dynamics of *Cryptococcus neoformans*-macrophage interactions reveal that fungal background influences outcome during cryptococcal meningoencephalitis in humans. mBio **2:**e00158-11. http://dx.doi.org/10.1128/mBio.00158-11.
35. **Alspaugh JA, Granger DL.** 1991. Inhibition of *Cryptococcus neoformans* replication by nitrogen oxides supports the role of these molecules as effectors of macrophage-mediated cytostasis. Infect Immun **59:**2291–2296.
36. **Granger DL, Hibbs JB, Jr, Perfect JR, Durack DT.** 1988. Specific amino acid (L-arginine) requirement for the microbiostatic activity of murine macrophages. J Clin Invest **81:**1129–1136. http://dx.doi.org/10.1172/JCI113427.
37. **Murray HW, Cartelli DM.** 1983. Killing of intracellular *Leishmania donovani* by human mononuclear phagocytes: evidence for oxygen-dependent and -independent leishmanicidal activity. J Clin Invest **72:**32–44.
38. **Salas SD, Bennett JE, Kwon-Chung KJ, Perfect JR, Williamson PR.** 1996. Effect of the laccase gene CNLAC1, on virulence of *Cryptococcus neoformans*. J Exp Med **184:**377–386. http://dx.doi.org/10.1084/jem.184.2.377.
39. **Walker L, Lowrie DB.** 1981. Killing of Mycobacterium microti by immunologically activated macrophages. Nature **293:**69–71. http://dx.doi.org/10.1038/293069a0.
40. **Rosen GM, Pou S, Ramos CL, Cohen MS, Britigan BE.** 1995. Free radicals and phagocytic cells. FASEB J **9:**200–209.
41. **Upadhya R, Campbell LT, Donlin MJ, Aurora R, Lodge JK.** 2013. Global transcriptome profile of *Cryptococcus neoformans* during exposure to hydrogen peroxide induced oxidative stress. PLoS One **8:**e55110. http://dx.doi.org/10.1371/journal.pone.0055110.
42. **Ding C, Yin J, Tovar EM, Fitzpatrick DA, Higgins DG, Thiele DJ.** 2011. The copper regulon of the human fungal pathogen *Cryptococcus neoformans* H99. Mol Microbiol **81:**1560–1576. http://dx.doi.org/10.1111/j.1365-2958.2011.07794.x.
43. **Ferreira T, Mason AB, Slayman CW.** 2001. The yeast Pma1 proton pump: a model for understanding the biogenesis of plasma membrane proteins. J Biol Chem **276:**29613–29616. http://dx.doi.org/10.1074/jbc.R100022200.
44. **Ioannoni R, Beaudoin J, Mercier A, Labbe S.** 2010. Copper-dependent trafficking of the Ctr4-Ctr5 copper transporting complex. PLoS One **5:**e11964. http://dx.doi.org/10.1371/journal.pone.0011964.
45. **Griffith OW, Bridges RJ, Meister A.** 1978. Evidence that the gamma-glutamyl cycle functions in vivo using intracellular glutathione: effects of amino acids and selective inhibition of enzymes. Proc Natl Acad Sci U S A **75:**5405–5408. http://dx.doi.org/10.1073/pnas.75.11.5405.
46. **Kumar A, Bachhawat AK.** 2010. OXP1/YKL215c encodes an ATP-dependent 5-oxoprolinase in *Saccharomyces cerevisiae*: functional characterization, domain structure and identification of actin-like ATP-binding motifs in eukaryotic 5-oxoprolinases. FEMS Yeast Res **10:**394–401. http://dx.doi.org/10.1111/j.1567-1364.2010.00619.x.
47. **Vallejo CG, Serrano R.** 1989. Physiology of mutants with reduced expression of plasma membrane H^+-ATPase. Yeast **5:**307–319. http://dx.doi.org/10.1002/yea.320050411.
48. **Lee SC, Kress Y, Zhao ML, Dickson DW, Casadevall A.** 1995. *Cryptococcus neoformans* survive and replicate in human microglia. Lab Invest **73:**871–879.
49. **Seider K, Brunke S, Schild L, Jablonowski N, Wilson D, Majer O, Barz D, Haas A, Kuchler K, Schaller M, Hube B.** 2011. The facultative intracellular pathogen *Candida glabrata* subverts macrophage cytokine production and phagolysosome maturation. J Immunol **187:**3072–3086. http://dx.doi.org/10.4049/jimmunol.1003730.
50. **Levitz SM, Nong SH, Seetoo KF, Harrison TS, Speizer RA, Simons ER.** 1999. *Cryptococcus neoformans* resides in an acidic phagolysosome of human macrophages. Infect Immun **67:**885–890.
51. **Vylkova S, Carman AJ, Danhof HA, Collette JR, Zhou H, Lorenz MC.** 2011. The fungal pathogen *Candida albicans* autoinduces hyphal morphogenesis by raising extracellular pH. mBio **2:**e00055-11. http://dx.doi.org/10.1128/mBio.00055-11.
52. **O'Meara TR, Xu W, Selvig KM, O'Meara MJ, Mitchell AP, Alspaugh JA.** 2014. The *Cryptococcus neoformans* Rim101 transcription factor directly regulates genes required for adaptation to the host. Mol Cell Biol **34:**673–684. http://dx.doi.org/10.1128/MCB.01359-13.
53. **Garcia-Hermoso D, Janbon G, Dromer F.** 1999. Epidemiological evidence for dormant *Cryptococcus neoformans* infection. J Clin Microbiol **37:**3204–3209.
54. **Gevaudant F, Duby G, von Stedingk E, Zhao R, Morsomme P, Boutry M.** 2007. Expression of a constitutively activated plasma membrane H^+-ATPase alters plant development and increases salt tolerance. Plant Physiol **144:**1763–1776. http://dx.doi.org/10.1104/pp.107.103762.
55. **Haruta M, Burch HL, Nelson RB, Barrett-Wilt G, Kline KG, Mohsin SB, Young JC, Otegui MS, Sussman MR.** 2010. Molecular characterization of mutant Arabidopsis plants with reduced plasma membrane proton pump activity. J Biol Chem **285:**17918–17929. http://dx.doi.org/10.1074/jbc.M110.101733.
56. **Goossens A, de La Fuente N, Forment J, Serrano R, Portillo F.** 2000. Regulation of yeast H^+-ATPase by protein kinases belonging to a family dedicated to activation of plasma membrane transporters. Mol Cell Biol **20:**7654–7661. http://dx.doi.org/10.1128/MCB.20.20.7654-7661.2000.
57. **Campetelli AN, Monesterolo NE, Previtali G, Santander VS, Amaiden MR, Arce CA, Valdez-Taubas J, Casale CH.** 2013. Activation of H^+-ATPase by glucose in *Saccharomyces cerevisiae* involves a membrane serine protease. Biochim Biophys Acta **1830:**3593–3603. http://dx.doi.org/10.1016/j.bbagen.2013.03.012.
58. **Luque-Ortega JR, Rivero-Lezcano OM, Croft SL, Rivas L.** 2001. In vivo monitoring of intracellular ATP levels in *Leishmania donovani* promastigotes as a rapid method to screen drugs targeting bioenergetic metabolism. Antimicrob Agents Chemother **45:**1121–1125. http://dx.doi.org/10.1128/AAC.45.4.1121-1125.2001.
59. **Perfect JR, Lang SD, Durack DT.** 1980. Chronic cryptococcal meningitis: a new experimental model in rabbits. Am J Pathol **101:**177–194.